RSC Advances

PAPER

View Article Online
View Journal | View Issue

Cite this: *RSC Adv.*, 2024, **14**, 10736

Fabrication of samarium doped MOF-808 as an efficient photocatalyst for the removal of the drug cefaclor from water

Anum Khaleeq,[a] Saadia Rashid Tariq *[a] and Ghayoor Abbas Chotana [b]

MOFs are emerging photocatalysts designed by tuning organic ligands and metal centers for optimal efficiency. In this study, a samarium decorated MOF-808(Ce) metal organic framework was fabricated by facile hydrothermal synthesis. The synthesized samarium decorated MOF-808(Ce) was characterized by using analytical techniques such as SEM, EDX, XRD and TGA to study its morphological, thermal and structural properties. SEM images showed that MOF-808(Ce) comprised of truncated octahedrons. The morphology of the material was changed upon Sm incorporation. Sm/MOF-808(Ce) exhibited better UV-vis light absorption properties than MOF-808(Ce) as evidenced by its slightly higher band gap value. This material was exploited for the degradation of the drug cefaclor from water. Cefaclor removal followed double a first order in parallel model (DFOP). Under UV light, 97.7% of the cefaclor was removed in only 20 minutes and after 60 minutes this removal efficiency was increased to 99.25%. These features exhibited that samarium decorated MOF has immense potential for the photocatalytic degradation of cefaclor as it generates e^- and h^+ to enhance the photocatalytic efficiency and it is a promising candidate to treat wastewater without formation of harmful byproducts.

Received 4th February 2024
Accepted 23rd March 2024

DOI: 10.1039/d4ra00914b

rsc.li/rsc-advances

1 Introduction

The introduction of various pollutants into the environment has badly affected the natural environment. These include pesticides, detergents, pharmaceuticals, food additives, agro-chemicals and various industrial effluents. Among these, pharmaceuticals are mostly non-biodegradable and persist for longer periods of time in water bodies.[1,2] They mainly comprise of nonsteroidal anti-inflammatory drugs (NSAIDs) β-blockers, antibiotics, contrast agents, vasodilators *etc.*[3] Hospitals, nursing homes and the pharmaceutical industry are major contributors to the entry of pharmaceuticals into wastewaters.[4,5] Similarly, aquaculture and animal husbandry are major sources of veterinary medicines in water bodies.[6,7] According to an estimate about 90% of the drugs administered to humans and animals are excreted and they find their way into sewage systems and ultimately reach freshwater bodies.[8] It is noteworthy that pharmaceuticals and specially antibiotics have been frequently detected in water samples.[9,10]

The emergence of these pharmaceuticals in wastewaters is associated with various health effects on non-target organisms such as endocrine disruption, behaviour changes *etc.*[11] Thus, it is important to explore efficient strategies for the removal of pharmaceuticals from wastewater before their disposal in freshwater bodies.[12–15] Advanced oxidation processes, including biological, chemical, or physical methods are used for the remediation of such pollutants.[16] Membrane technology has also been used but it consumes more energy, can be contaminated easily, and needs more cost.[17] Recently, photocatalysis has gained importance for the degradation of pollutants as it is high in performance, ecologically benign, works at ambient temperature and pressure and causes no secondary waste formation.[18] Removal of pollutants by photo-catalysis is cost-effective and sustainable as compared to other treatment methods that require significant energy input.[19]

A number of materials like co-ordination complexes, metal organic framework (MOFs), covalent organic polymers (COP) and porous aromatic framework (PAF) can be used for as photo-catalysts. MOFs have emerged as highly efficient materials for the degradation and abatement of pollutants.[20–23] Like heavy metals, antibiotics, dyes, inorganic ions, and radio nuclei *etc.*[24–27]

In 2021, Kaur *et al.* used the MOF to degrade ofloxacin. A 72 percent degradation was reported in the visible light within 3 hours.[28] MOFs may also exhibit ligand–metal charge transfer under light exposure. This type of MOF has been used for the visible light assisted degradation of hydrogen peroxide (H_2O_2). Furthermore, mechanism for the degradation of organic pollutants was also described.[29]

Usually, the process of catalysis and adsorption of pollutants tends to be immediate and inseparable processes. In

[a]*Department of Chemistry, Lahore College for Women University, Jail Road, Lahore, 54000, Pakistan. E-mail: saadiartariq@yahoo.com*

[b]*Department of Chemistry and Chemical Engineering, Syed Babar Ali School of Science & Engineering (SBASSE), Lahore University of Management Sciences (LUMS), Lahore 54792, Pakistan*

photocatalytic degradation, the pollutants first interact with porous structural network of MOF or MOFs composites and then reacts with the active species of the framework. This process is followed by chain of UV-visible light driven catalytic degradation reactions.[30]

For photocatalytic processes, MOFs are used on semiconductor precursors and that can be composited with conventional semiconductor materials. MOF based materials have large light harvesting abilities which is attributed to high porosity and interconnected channels of metal–ligand framework. This enhances electron transfer efficiency and reduces recombination of photoinduced e^-/h^+ pairs. The core active radicals in photodegrading organic pollutants are mainly $O^\bullet$ and $OH^\bullet$ and oxidation holes. They are produced by photogenerated e^- and h^+ active radicals in photodegrading organic pollutants are mainly $O^\bullet$ and $OH^\bullet$ and oxidation holes. They are produced by photogenerated e^- and h^+.[31]

MOF-808(Ce) is a highly porous structure with high surface area and higher mechanical and thermal stability. These features make it a highly effective material for adsorptive degradation of pollutants. Moreover, its synthesis is facile[32] and, it may be decorated with lanthanides like samarium in a very simple way, to improve the separation of charges and reduce the bandgap.[33–36] It has higher central metal atom oxidation state and high stable porosity. It possesses excellent photocatalytic properties for wastewater purification.[37] Its proposed structure is provided in Fig. 1a.

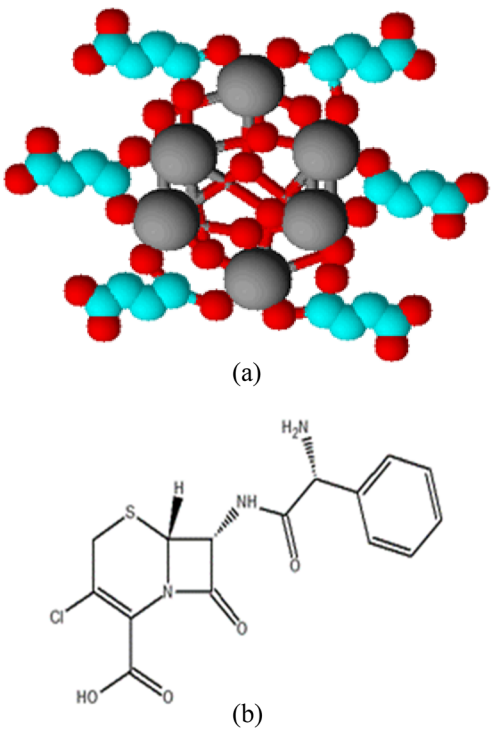

Fig. 1 (a) Proposed 3-D structure of Sm/MOF-808(Ce). The blue, dark red, and greyish spheres indicate carbon, oxygen, and metals, in their respective order. Hydrogen atoms are omitted for clarity. (b) Chemical structure of cefaclor ($C_{15}H_{14}ClN_3O_4S$).

Sm doped MOF-808(Ce) was used for the photodegradation of cefaclor a widely used pharmaceutical belonging to the cephalosporin class. The IUPAC name of cefaclor is (6*R*,7*R*)-7-[(2*R*)-2-amino-2-phenylacetyl]amino-3-chloro-8-oxo-5-thia-1-azabicyclo oct-2-ene-2-carboxylic acid (Fig. 1b). It is commonly used for the treatment of various diseases. Therefore, it frequently enters the water bodies and soil through sewers. It has also been found that its transformation products are more toxic than the drug itself.[38] Thus, in order to avoid its harmful effects on human health, it is imperative to find a cost effective and efficient method for its removal from water bodies. It is expected that the Sm decorated MOF will act as an efficient photo-catalyst for the degradation of cefaclor without production of any toxic intermediates of photodegradation.

2 Materials and methods

2.1 Quality assurance

All reagents and chemicals used in this work were of analytical grade and used as delivered. Cerium ammonia nitrate (>99.5% metal basis) and HCl were purchased from Merck, trimesic acid (>98%, H_3BTC, Germany), dimethylformamide (DMF 98%) and ethanol were procured from Sigma-Aldrich. Doubly distilled water prepared by Milli-Q was used throughout the study. Calibration of volumetric apparatus was performed prior to use. The high quality and acid resistant borosilicate glass was used through the experiment.

2.2 Synthesis of MOF-808(Ce) and Sm/MOF-808(Ce)

MOF-808(Ce) was prepared by modulated hydrothermal procedure adapted from literature.[39] The MOF was synthesised by constant stirring of Ce(IV) ammonium nitrate as central metal precursor and trimesic acid as the organic linker in DMF (98%) and formic acid (1 : 1 v/v) at 135 °C for 40 minutes. For preparing the Sm decorated MOF, the solution of samarium nitrate prepared in water/citric acid mixture was added to MOF solution while maintaining Sm : Ce ratio of 1 : 9. The contents were sonicated and transferred to a stainless-steel autoclave (Teflon-lined) of 100 mL capacity for 14 hours of heating at 130 °C. The prepared MOF-808 and Sm/MOF-808 were analysed by using various techniques such FTIR, XRD, SEM-EDX *etc.* The thermal stability of synthesized compounds was analysed by using TGA analysis.

2.3 Photocatalytic degradation of cefaclor

For determining the photocatalytic degradation of cefaclor by using MOF-808(Ce) and Sm/MOF-808(Ce), stock solution of cefaclor was prepared at 100 mg L^{-1} concentration and used with appropriate dilution. For a typical degradation experiment, the 100 mL of drug solution added with a certain amount of catalyst (MOF-808(Ce) or Sm/MOF-808(Ce)) maintained at an optimum pH 4 was irradiated with light for different time intervals. The pH of drug solutions was maintained by using 0.01 M NaOH and 0.01 M HCl solutions in the range of 1 to 11 to study the effect of pH on photodegradation. Before irradiation, the solutions were stirred continuously for 30 minutes under

dark environment at room temperature to attain the adsorption–desorption equilibrium. To study the photodegradation performance of prepared materials, the experiments were carried out under ultraviolet radiation (280 nm) as well as visible light (446 nm) by using UVC tubes with maximum output at a wavelength of 280 nm or tungsten bulb with a maximum output at a wavelength of 446 nm. The intensity of UV light was 0.96 mW cm^{-2} while that of visible light was 8.5 mW cm^{-2}.

A self-designed reactor was used for carrying out the photodegradation steps. The source of light here was positioned above the glass reactor of volume 300 mL. The distance between the reactor and light source was kept at 15 cm. The water was kept circulated beneath the reactor to get rid of any heat produced during light irradiation. The reactor was also equipped with a fan to remove the gaseous products produced during the experiment. The continuous stirring of reaction contents was carried out by using a magnetic stirrer. After light irradiation for a particular time interval, the aliquots of sample solutions were removed to determine the left-over concentration of drug in the solution by using a UV visible spectrophotometer. The concentration of cefaclor is proportional to its absorbance therefore the changes in drug removal were tracked at 266 nm which is the λ_{max} of cefaclor. The degradation efficiency was determined by eqn (1) as given below:

$$\text{Percentage degradation (\%)} = (C_0 - C_t)/C_0 \times 100 \quad (1)$$

Here, C_0 is the initial concentration (mg L^{-1}) before illumination, while C_t is remaining concentration of drug after degradation. The effect of different factors such as adsorbent dose, time and cefaclor concentration were also studied for optimization. For studying the effect of catalyst dose, the amount of catalyst was varied between 0.01–0.1 g/100 mL while the effect of pH was studied by carrying out experiments at pH 1–10.

2.4 Reusability and stability studies

Reusability of the prepared catalysts was checked for four consecutive cycles after use. A 0.05 g of photocatalyst was added to 100 mg L^{-1} drug solution maintained at 303 K and a pH of 4 and irradiated for 30 minutes. After use, the catalyst was recovered by centrifugation, washed successively with distilled water and dried in an oven at 80 °C. The used catalyst was characterized by SEM, EDX and XRD analyses to look into any structural collapse that might occur after use. The drug solution after photodegradation experiments were checked for the leached Ce or Sm metals from MOF structure by spectrophotometer using *ortho*-phenylenediamine and HCl as coloring agent.

2.5 Scavenging studies

In order to identify the main active species involved in the photodegradation process of cefaclor by prepared material, the experiments were performed with addition of different scavengers. For this purpose, a 1 mM solution of scavenger was added before turning on the light source on the drug solution maintained at optimum conditions, and the efficiency of catalyst was determined in the presence of scavenger by using UV-visible spectrophotometer. Scavengers used included: isopropyl alcohol, $K_2Cr_2O_7$, *p*-benzoquinones and formic acid to quench $OH^{\bullet -}$, e^-, $O^{\bullet -}$ and h^+ respectively.

2.6 Photodegradation of cefaclor in the real water samples

Photodegradation studies of cefaclor were performed for real sample containing the other drugs as well to evaluate the efficiency of photo-degradation by using synthesized catalyst under optimum conditions. In these experiments, the sample was analysed by HPLC equipped with UV detector. The chromatographic analysis was carried out on HPLC-UV designed with a vacuum degasser. A C-18 column (254 mm × 4.4 mm ID, 5 m) kept at ambient temperature (25 °C) was used. The mobile phase was (5–10%) acetonitrile, 0.1% water and formic acid with flow rate of 1.5 mL min^{-1}, an injection volume of 5 μL. Cefaclor residues were detected at 266 nm with retention time of 3.328 min., along with famotidine at 1.028 min and chlorpheniramine at 1.755 min. The 0.1 g of catalyst and effluent were irradiated with UV and visible light for 30 minutes with constant stirring. Filtered solutions were run on HPLC.

2.7 Band gap measurement

The optical band gap energy of MOF was estimated from absorption spectra using Wood–Tauc plot ($h\nu$) *versus* $(\alpha h\nu)^2$. The mechanism of photodegradation was evaluated by using the band gap energies and shift in wavelengths of maximum absorption.

3 Results and discussion

The residues of pharmaceutical drugs present in river water and freshwater resources pose a remarkable health risk to the exposed populations due to their adverse effects.[40] Thus, MOF-808(Ce) was employed for removal of cefaclor from aqueous solution.

Sm doped MOF-808 comprises of the trimesate linkers connected to cerium-samarium nodes (secondary building unit) in the metal organic framework. Formate anions as modulators balanced the charge on the synthesized framework. Dimethyl formamide was selected as solvent because it has a high polarity of 6.4, good synthetic yield, thermal stability, and wide range of solubility. The details of materials characterization and their use as a photocatalyst are provided in the forthcoming sections:

3.1 Characterization of MOF-808(Ce) and Sm/MOF-808(Ce)

MOF-808(Ce) and its modified form were characterized by different analytical techniques including SEM, TGA, FT-IR, UV-visible spectroscopy and XRD.

The morphology of MOF-808(Ce) and Sm/MOF-808(Ce) was studied by scanning electron microscope as shown in Fig. 2a and b. The figure showed that MOF-808 particles comprised of truncated octahedrons. Upon functionalization with Sm, a significant change in the morphology of the particles was observed in SEM images. SEM image of MOF-808(Ce) showed rod like morphology while after doping it changed to regular

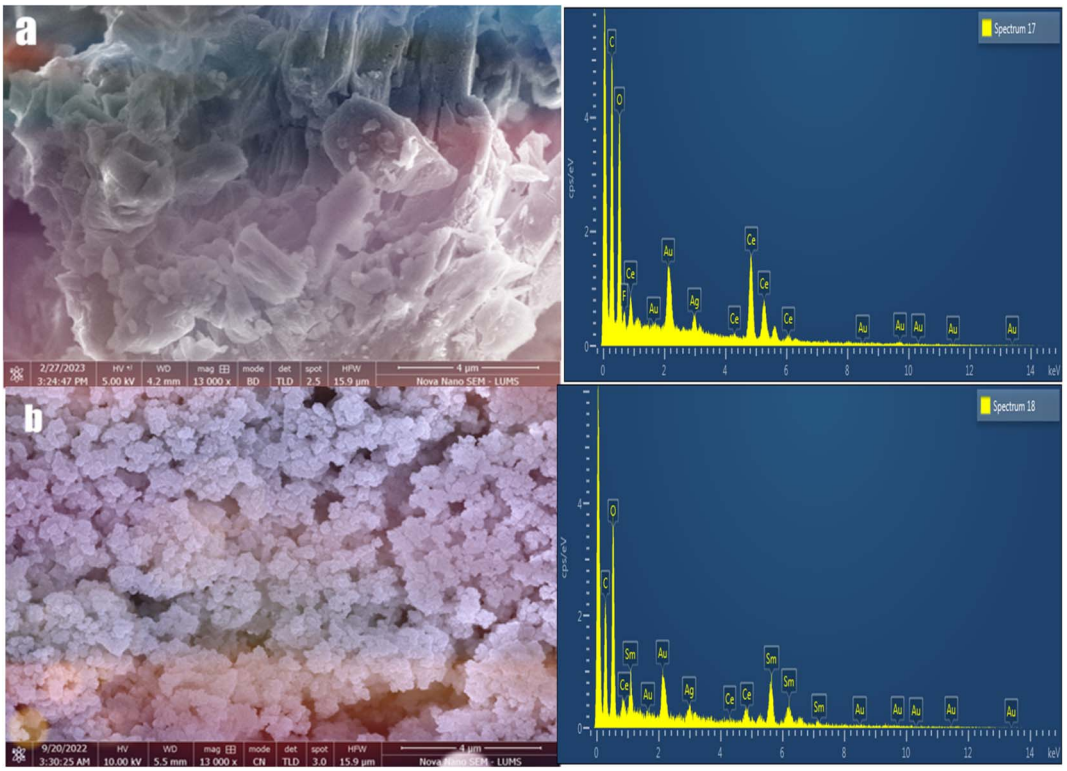

Fig. 2 Scanning electron micrographs and EDX images of MOF-808(Ce) (a) and Sm/MOF-808(Ce) (b).

crystal grains. The MOF particles exhibited the size in the range of 65–164 nm as determined by Image J 1.53o software.[41,42]

Distribution of pristine and functionalized MOF was studied by EDX mapping. Fig. 2 indicated that samples contained C, O, Sm and Ce elements. Well resolved peaks in the EDX spectra were associated with metallic elements *i.e.*, cerium and samarium. According to atomic percentage obtained from SEM-EDX, the empirical formula was estimated as $Ce_{1.33}C_{1.40}$-O(OH)(BTC) for MOF-808(Ce) and $Sm_1Ce_{6.04}C_{10}O(OH)$(BTC) for Sm/MOF-808(Ce). The percentages matched well with previously reported literature.[43]

To gain understanding of binding modes, FTIR spectra were recorded at 298 K in the wavenumber range of 500–4000 cm^{-1}. Fig. 3 a depicts the FTIR spectrum of MOF-808(Ce) and Sm/MOF-808(Ce). Characteristics bands appeared in the region of 1612–1550 cm^{-1} and 1435–1369 cm^{-1}. These bands are related to the stretching asymmetric vibrations of carboxylate ions (–COO–) and symmetric Ce–O vibrations respectively. The presence of these bands confirmed the coordination of cerium ions with 1,3,5-H_3BTC. The OH-groups are associated with broad band at 3415 cm^{-1}. The vibrations observed at 1337 cm^{-1} and 1440 cm^{-1} were attributed to aromatic rings of BTC moieties. Moreover, vibration at 1391 cm^{-1} showed the Sm doping in case of Sm/MOF-808(Ce). In the FTIR spectra of MOF-808(Ce), the peaks of carboxylic acids were not observed, as carboxyl groups in the MOF were consumed during the synthesis, for the growth of MOF-808(Ce). Strong vibration of Ce–O observed at 691 cm^{-1} confirmed the coordination of carboxyl groups with cerium ion in BTC.

The thermal stability exhibited by MOFs is depicted in Fig. 3b in terms of TGA curves. TGA curve for pristine MOF exhibited three steps for mass loss with increasing temperature. The first mass loss of about 20% occurred below 200 °C. This was due to the removal of guest solvent molecules.[44] A further 5% mass loss occurred at 300 °C that was attributed to the decomposition of MOF with the release of backbone fragments as demonstrated by the exothermic process of thermal decarboxylation. This Fig. 3b showed an endothermic peak only in dry air conditions at 370 °C confirming dehydration probably because of phase change of pristine MOF to amorphous form.

At 450 °C, the final step of decomposition occurred that corresponded to the loss of inorganic oxides and carbonates. The consistent mass loss curve represented the decomposition of metal organic framework.[45] TGA data of functionalized MOF showed a continuous weight loss up to 380 °C. This temperature is ascribed to the removal of solvent, water, and collapse of framework with formation of inorganic oxide as well as organic species. The structural collapse temperature for pure MOF was greater than that of doped MOF.

Fig. 3c depicts the PXRD patterns of MOF-808(Ce) and Sm/MOF-808(Ce) having peaks at different 2θ values *i.e.*, 10.4°, 10.8°, 13.76°, 20.9°, 28.08° corresponding to (100), (110), (110), (210) and (211) crystal planes. The relative crystallinity of pristine and modified MOF was analysed by using Origin Pro software after baseline correction. By increasing the content of samarium, the peaks of MOF-808(Ce) were decreased in intensity. But they showed the interaction of Ce with linker even after samarium doping. Phase purity was explained by the

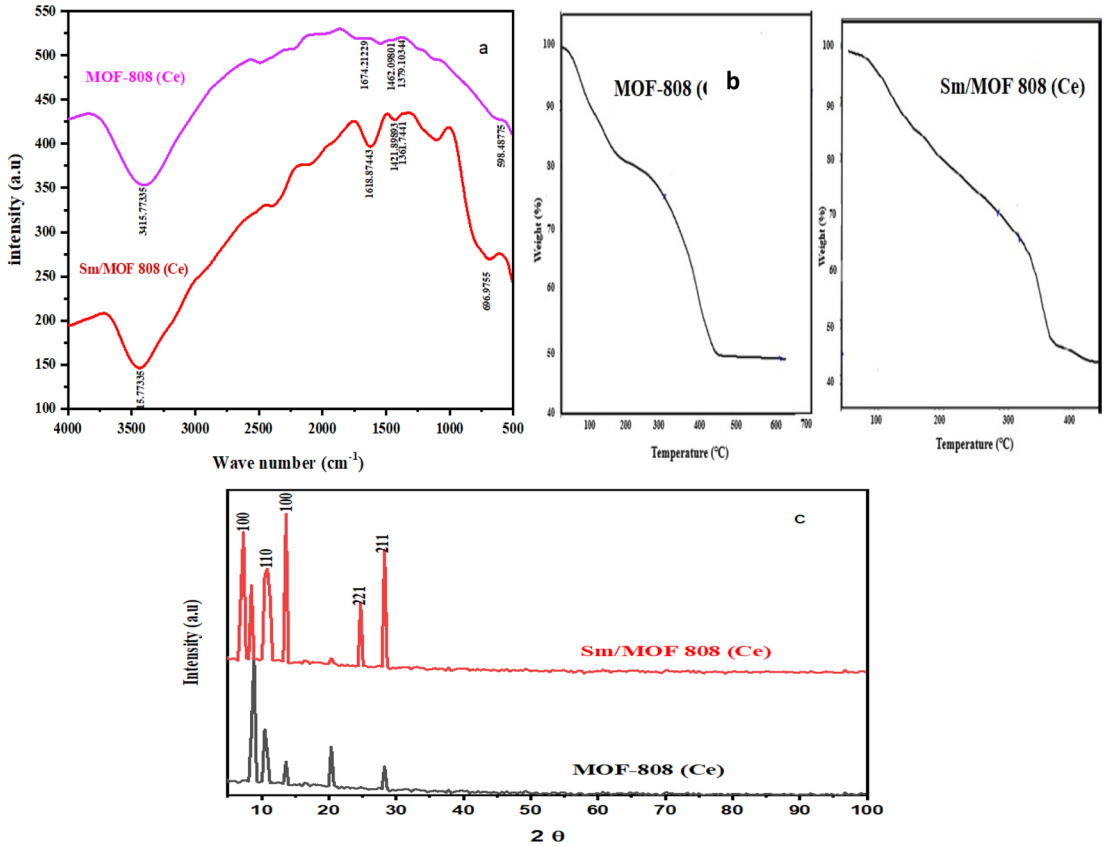

Fig. 3 FTIR spectra (a) thermal analysis (b) and XRD patterns (c) of MOF-808(Ce) and Sm/MOF-808(Ce).

resemblance between the positions of peaks. In terms of positions of peak and relative intensity, diffractogram resembled with the UTSA-120a crystalline material as reported in literature.[43] MOF-808(Ce) exhibited cubic crystal shape with group *Fd*3*m* having lattice parameter $a = 35.076(1)$ Å. Three-dimensional networks existed in MOF-808(Ce) with spn topology. Internal diameter was 4.8 Å with tetrahedral cages. Large adamantine was thus designed with 18.4 Å diameter of internal pore (JCPDF 08-0234).[46] The indexing of XRD patterns was further carried out using X-pert Pro software.

3.2 Removal of cefaclor by using MOF-808(Ce) and Sm/MOF-808(Ce)

The pristine and Sm modified MOF-808(Ce) were studied for their potential to remove cefaclor drug. Different factors were optimized including pH, time of contact, initial concentration of drug, dose of MOF material and temperature.

Photocatalytic efficiency of MOF depends upon the pH of solution. The pH can affect the oxidative property of produced reactive radicals. With a change in pH, there will be a change in the surface charge of catalyst molecules thereby altering the degree of ionization.[47] As shown in Fig. 4a the drug degraded by MOF and Sm doped MOF was significantly decreased at pH of 10 and 1, which is similar to previous literature.[48] This tendency is attributed to the deportation of drug at high pH (pK_a of cefaclor is 1.5) and decrease of surface charge of MOF-808(Ce) and destruction of its structure at low pH. In other words, repulsive interactions between MOF and cefaclor were increased at very low pH.

Under visible and UV light, the photodegradation capacity was decreased to 0.0833% for Sm/MOF-808(Ce) as pH dropped from 4 to 1. At low pH values the H^+ competes with drug ions.[49,50] The maximum cefaclor removal was obtained at the pH of 4.0 under both visible and UV lights *i.e.*, 51.75% and 97%, respectively. Previous research also reports pH 4 as optimum pH for photodegradation of drugs. Different functional groups like –OH, –NH, C=O on cefaclor react with oxygen containing groups present on the MOF surface. Resultantly, hydrogen bond formation would lead to increased drug adsorption followed by its increased degradation. Enhanced removal of cefaclor under UV light was attributed to the high distribution of cefaclor ions as the monochromatic absorption coefficient of cefaclor is high at pH 4. Many studies have proved that UV light absorbance and photolytic properties are influenced by distribution of ions. Thus, at different pH values, different protonated and deprotonated forms of cefaclor exist that affect its degradation.[51] Furthermore, at acidic pH the concentration of H^+ ions caused greater production of hydroxyl radicals resulting in high photodegradation of cefaclor. In alkaline media, the number of negatively charged sites were increased leading to electrostatic repulsion and thus poor drug degradation. With the increase in the number of insoluble ions produced, the intensity of light transmitted was also reduced that prevented the production of

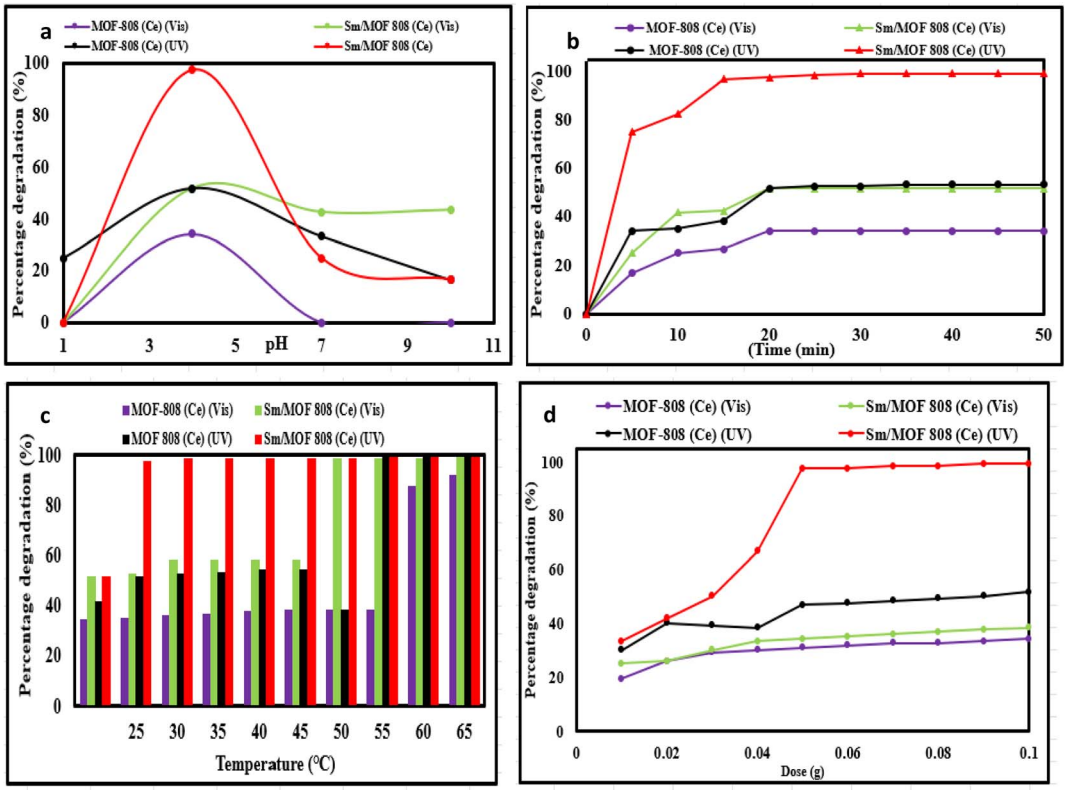

Fig. 4 Effect of pH (a), time (b), temperature (c) and catalyst dose (d) on cefaclor removal by MOF-808(Ce) and Sm/MOF-808(Ce).

hydroxyl radicals and hence photodegradation rate was lowered.[52]

An increase in the amount of drug removed was observed by increasing the contact time of catalyst with drug as depicted in Fig. 4b. It was observed that the photodegradation was increased until all the active sites of catalyst were occupied. At 30 °C and pH 4, 100 mg catalyst was used with different solutions. Initially the drug removal was enhanced with time as the number of active sites were vacant and available on catalyst due to its large surface area. So, 51.75% of cefaclor was degraded within the first 20 minutes by pristine MOF-808(Ce) whereas Sm/MOF-808(Ce) removed 97.58% of cefaclor in this time under UV light.

These results suggested that under UV light aggregation was prevented and MOFs showed increased UV light absorption and reduced decomposition by maintaining its crystallinity. Ultraviolet light generates cluster defects in the nanoregions of MOFs, so abundant catalytic sites were available in doped MOF that attracted drug molecules to the surface of MOF as compared to pristine MOF.[53] Fig. 4c depicts the temperature effect on removal of cefaclor. It is apparent from the figure that photocatalytic degradation was increased with the gradual rise in temperature. As, the activation energy barrier was overcome from the energy generated with temperature rise.[54] In particular, the photocatalytic performance of MOFs was more sensitive to temperature, and their degradation efficiencies reduced from 30 to 90 percent because of structural degradation of MOFs and drug at higher solution temperatures.

Another parameter that influenced the photodegradation efficiency was the photocatalyst dose. The results depicted in Fig. 4d, indicated that photocatalytic degradation was higher at low catalyst dose. When the dose was increased from 0.01 to 0.1 g, the drug degradation rate was initially increased as the drug molecules rapidly occupied the sites present on surface of photocatalyst.

The photocatalytic efficiency gradually decreased as the excess photocatalyst competed for available photons resulting in particle aggregation and subsequently decreasing degradation. The aggregation also decreased the surface area of photocatalyst resulting in lack of active sites.[55] A catalyst dose of 0.1 g for MOF-808(Ce) and 0.05 g for Sm/MOF-808(Ce) were selected for further photodegradation experiments.

Photocatalytic performance of both the catalysts was reduced in visible light. This decline in visible light is due to scattering of low energy visible light by increased in number of photocatalytic particles. Whereas as UV light has less wavelength and high energy so the probability of reaction between drug and oxidizing species is increased that promotes the production of hydroxyl radicals on catalyst surface which leads to improvement of photocatalysis in ultraviolet light.[56]

3.3 Stability and reusability of photocatalyst

Cost of the catalyst is considerably reduced if it is reuseable for successive cycles.[57,58] So stability and recyclability of the prepared catalyst was determined while treating actual waste water. The recyclability of MOFs was checked for three

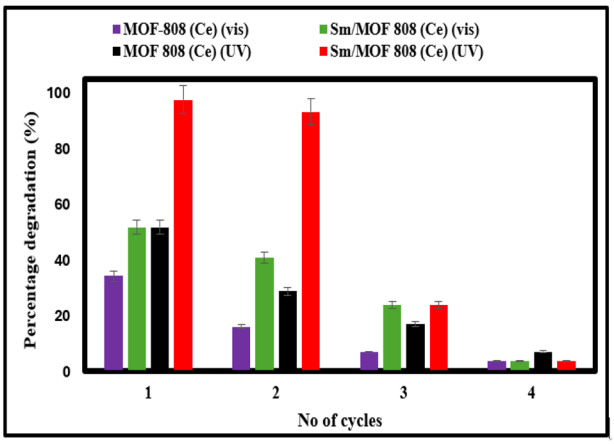

Fig. 5 Reusability and stability MOF-808(Ce) and Sm/MOF-808(Ce).

consecutive cycles after use as shown in Fig. 5. It was observed that drug degradation efficiency was not decreased upto two cycles. When MOF was used in the first cycle, 97.6% removal of drug was observed. The MOF's efficiency was slightly reduced in the second cycle due to a reduction in number of active sites that were collapsed. At third cycle 23% removal was still achieved which further declined in fourth cycle. The decreased efficiency was attributed to the collapse of active sites available on the surface of MOF.

The number of active sites were also reduced to a greater extent due to trap of drug molecules with in the pores of MOF structure during fourth cycle which were not recovered even after washing. So the efficiency during the fourth cycle was negligible for drug removal.

In order to determine the structural deformation of catalysts after reuse in consecutive cycles, the XRD and SEM analysis were carried out again after use and corresponding data is depicted in Fig. 6a–c. The SEM images showed that the morphology of the pristine and Sm doped MOF was affected after reuse due to formation of aggregates.

The Fig. 6c, for XRD analysis showed that intensity and position of XRD diffraction peaks were slightly changed after reuse thereby confirming that the structure of the catalyst was retained after photocatalytic degradation cycles.

3.4 Mechanism of photocatalysis

MOFs absorb over wide range in UV-visible spectrum as shown in the diffraction reflection spectrum (DRS), Fig. 7a. The abortion maximum of MOF-808(Ce) is at 358 nm that is red shifted in doped MOF to 379 nm suggesting both MOFs as potential absorber for solar light especially in UV-visible range. MOF-808(Ce) showed narrow absorption from 300–500 nm, while Sm/MOF-808(Ce) has wider absorption range from 300–570 nm therefore its optical absorption capacity is broader depicting it to be an efficient photo-catalyst.

The equivalent absorption coefficient was determined using the Kubelka–Munk eqn (2)

$$\alpha h\nu = A(h\nu - E_g)^n \quad (2)$$

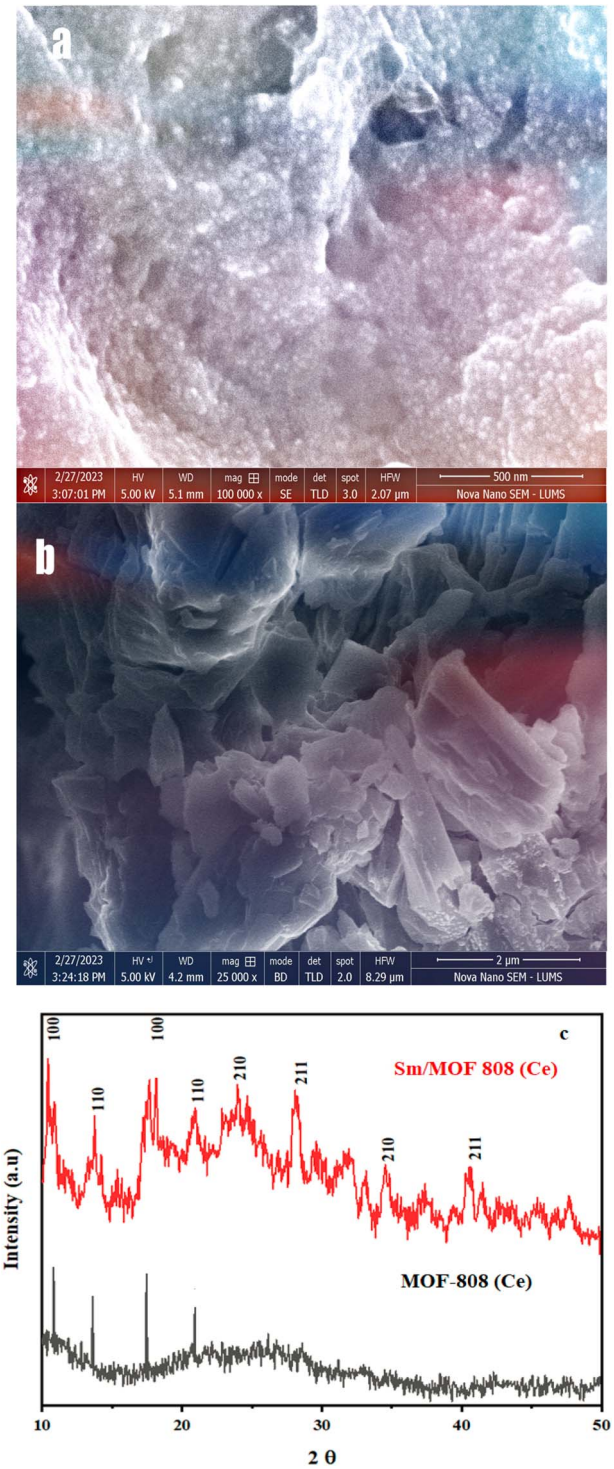

Fig. 6 SEM micrographs (a) and (b) and XRD patterns (c) of MOFs after photocatalytic experiments.

where, h is Planck's constant (6.626×10^{-34} J s), A is a proportionality constant, α is coefficient of absorption. E_g is the band gap, ν is frequency of light and $h\nu$ is the energy of the photons. Optical band gap energies of MOFs were estimated from absorption spectra using Wood–Tauc plot ($h\nu$) *versus* $(\alpha h\nu)^2$ and was found to be narrow *i.e.*, 1.76–1.81 eV as shown in

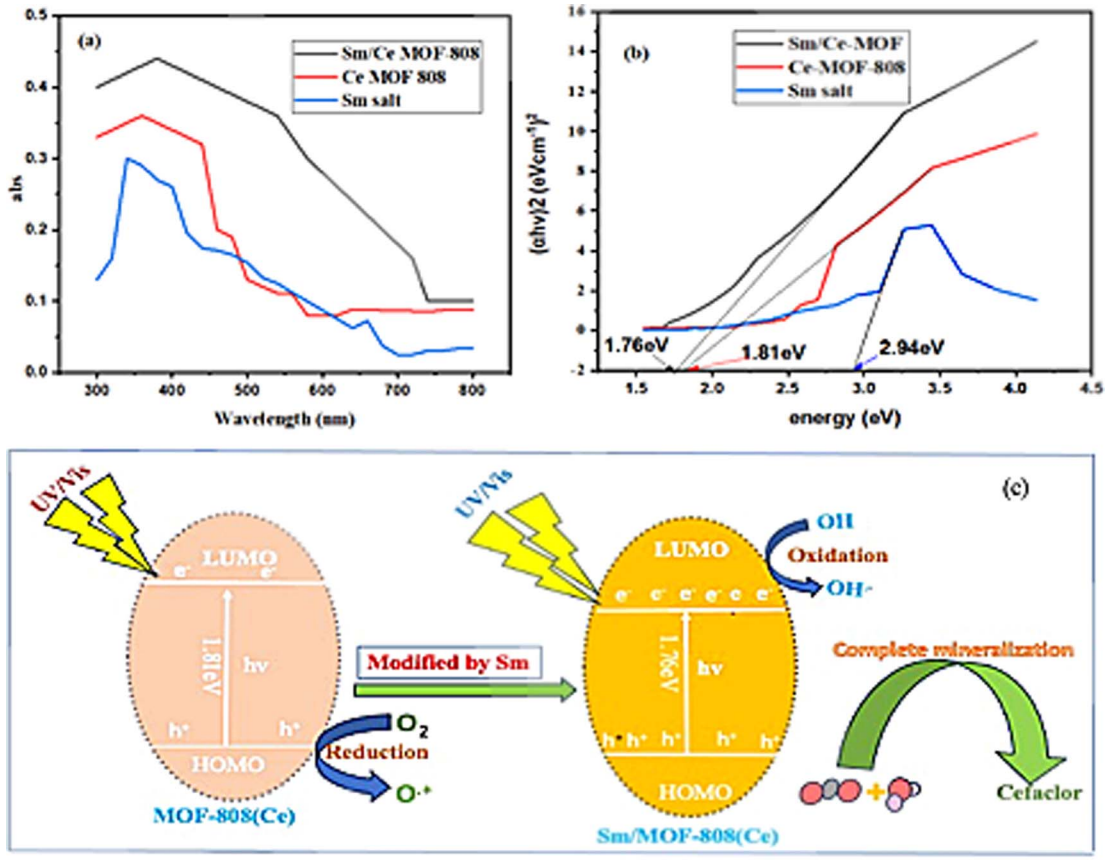

Fig. 7 UV-vis DRS spectra (a) Tauc plots (b) for estimation of band gaps and proposed scheme (c) for removal of cefaclor in the presence of MOFs.

Fig. 7b. Small band gaps enable visible light excitation in MOFs. Less electrons and hole recombination will limit the generation of oxidizing species/radicals. This could be resolved by reduction of particle dimensions making it suitable for catalytic reactions.[59,60]

The absorbance of MOF-808(Ce) was less than doped Sm/MOF-808(Ce) as HOMO–LUMO gap of pristine MOF-808(Ce) (1.81 eV) is large. MOFs photocatalyst possess the metallic chains that help in capturing visible photons and generate electron–holes in the process. Both catalysts displayed high absorption in UV and visible light.

The conduction band (ECB) and valence band (EVB) potential of MOF and MOF derived material were calculated theoretically by Mulliken electronegativity theory using following equations:

$$E_{CB} = x - E_e - 0.5E_g \quad (3)$$

$$E_{VB} = E_{CB} + E_g \quad (4)$$

where, E_g is the band gap of the semiconductor material and E_e is taken as 4.5 eV which comes from the energy of free electrons. Moreover, w is the electronegativity of the semiconductor. w is calculated by the geometric mean of the absolute electronegativity of the constituent elements. E_{VB} is VB potential and E_{CB} is CB potential.[61]

The proposed degradation scheme as shown in Fig. 7c comprised of excitation of the CB e^- in Sm; then these photogenerated electrons migrate to the less negative CB of MOF-808(Ce) and thus lifetime of charge carriers was prolonged. These charge carriers together with the e^- of the conduction band of the cerium MOF-808 reacted with the surface O_2. Considering standard redox potential superoxide $^{\bullet}O_2^-$ radicals are generated because of negative nature of the CB edge potential in contrast to the standard redox potential of O_2/O_2. Then, the $^{\bullet}O_2^-$ degraded cefaclor. The h^+ of the MOF-808(Ce) were transmitted to the VB of the samarium.[62] This increased the photocatalytic performance because generated holes in the VB of samarium are found to react with $OH^{\bullet-}/H_2O$ to produce OH. This reaction is credited to more positive nature of the VB edge potential than the standard redox potential of OH/OH^-. By substitution of samarium in MOF-808, LMCT is markedly improved because carboxylate linker also transfers electrons to the metal clusters. The overlapping d orbitals of samarium and cerium metals and pi orbitals in organic ligand BTC allowed efficient transfer of photogenerated electrons. Here, the cefaclor reacted with h^+ and generated the cefaclor intermediate and finally, complete mineralization was achieved.[63] From the discussion, it is apparent that the photocatalysis mechanism was mainly due to interfacial transfer of charges that was triggered in fabricated MOF under irradiation.[64]

Comprehensively, the resultant reactions generated $^{\cdot}O_2^-$ and h^+ favouring the photodegradation process. The fabricated MOF material turns out to be more dynamic catalytic centres for attachment of cefaclor and its subsequent removal from wastewater. Therefore, high-quality interfaces in the hetero-structure composites played a significant role in improving the photo-catalytic performance as depicted in eqn (5) through (10)

$$\text{Photocatalyst MOFs} + h\nu\ (\text{UV/vis}) \rightarrow h^+_{VB} + e^-_{CB}\ (\text{electrons}) \quad (5)$$

$$h^+_{VB} + H_2O \rightarrow {}^{\cdot}OH + H^+ \quad (6)$$

$$^{\cdot}O_2\ (\text{catalyst surface}) + e^-_{CB} \rightarrow {}^{\cdot}O_2^- \quad (7)$$

$$^{\cdot}O_2^- + H^+ \rightarrow (^{\cdot}OOH)_{ads} \quad (8)$$

$$2{}^{\cdot}OOH \rightarrow {}^{\cdot}O_2 + H_2O_2 \quad (9)$$

$$H_2O_2 + h\nu \rightarrow 2{}^{\cdot}OH \quad (10)$$

$$\text{Organic pollutant (cefaclor)} + (^{\cdot}OH,\ h^+_{VB},\ e^-_{CB} \text{ or } {}^{\cdot}O_2^-) \rightarrow H_2O + CO_2\ (\text{complete mineralization})$$

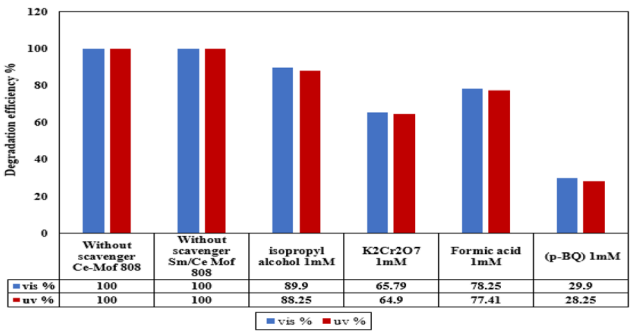

Fig. 8 Photocatalytic degradation of cefaclor in the presence of different scavengers.

3.5 Scavenger studies

As stated in the above mechanism the dominant species responsible for the photo-assisted removal of cefaclor could be superoxide and hydroxyl radical in addition to e^- and/or holes as depicted in Fig. 8. To provide insight into the role of these species in degradation of cefaclor with the photocatalyst, different experiments were conducted using various scavengers. Scavengers selected were *p*-benzoquinone (*p*-BQ) for trapping of superoxide radicals ($^{\cdot}O^{2-}$), iso-propyl alcohol for hydroxyl radicals ($^{\cdot}OH$), $K_2Cr_2O_7$ for (e^-) and formic acid for holes (h^+). The initial concentration of the scavengers was 1 mM. Fig. 8 depicts the degradation of cefaclor in the presence of different scavengers. It elaborates that all the reactive species contributed

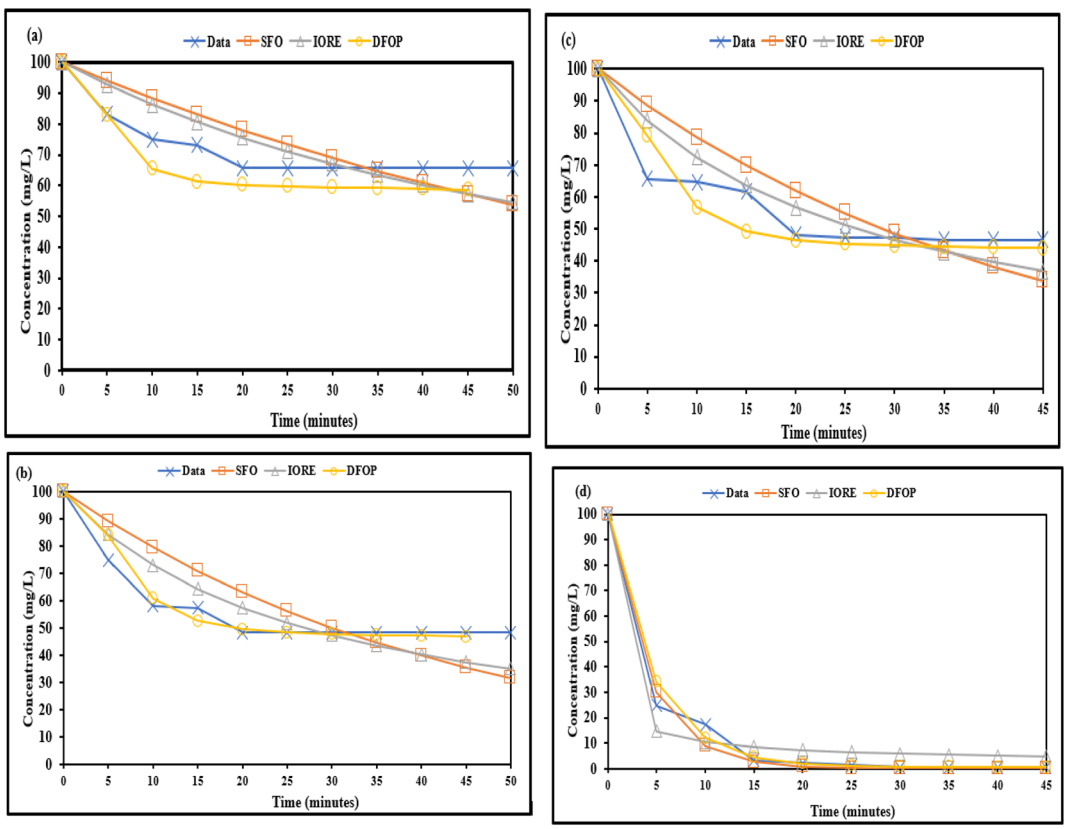

Fig. 9 Kinetics of photocatalytic degradation of cefaclor in the presence of (a), MOF-808 (Ce) in visible light (b), Sm/MOF 808 (Ce) in visible light (c), and MOF-808 (Ce) in UV radiation (d) Sm/MOF 808 (Ce) in UV radiation.

Table 1 Kinetic parameters of different degradation models for the removal of cefaclor by using the synthesized MOFs

		Visible		Ultraviolet	
Model	Parameters	MOF-808(Ce)	Sm/MOF-808(Ce)	MOF-808(Ce)	Sm/MOF-808(Ce)
SFO	K	0.0124	0.023	0.024	0.24
	S_{SFO}	849.7	1641	1545	103.3
	DT_{50}	55.80	30.11	28.85	2.888
	DT_{90}	185.4	100.0	95.82	9.59
IORE	K_{IORE}	0.00036	0.00037	0.00038	0.00048
	N_{IORE}	1.820	2.000	2.000	2.980
	S_{IORE}	633.0	827.2	790.8	317.6
	DT_{50}	59.40	26.95	26.25	0.339
	DT_{90}	435.1	242.6	236.2	10.88
	T_{IORE}	130.9	73.01	71.11	3.275
DFOP	K_1	0.300	0.210	0.220	0.220
	K_2	0.00085	0.001	0.001	0.00079
	S_{DFOP}	4196	2518	432.0	119.5
	$1DT_{50}$	2.310	3.320	3.160	3.150
	$2DT_{50}$	815.5	693.2	693.2	87.74
	G	0.5	0.5	0.5	0.5
Critical value	S_c	1038	1094	1045.8	436.1

to the degradation process. *p*-BQ showed the most vital impact on the catalytic process. The catalytic performance is mainly suppressed by pBQ so the superoxide radicals ($^{\bullet}O^{2}$) appeared as the most likely active species in the cefaclor degradation.

3.6 Kinetics of photodegradation

Further insight into the mechanism of degradation was gained by using different kinetic models. Three models used were: single first order rate model (SFO), indeterminate order rate equation (IORE) and double first order in parallel model (DFOP) as shown in Fig. 9. Kinetic studies data for MOFs assisted

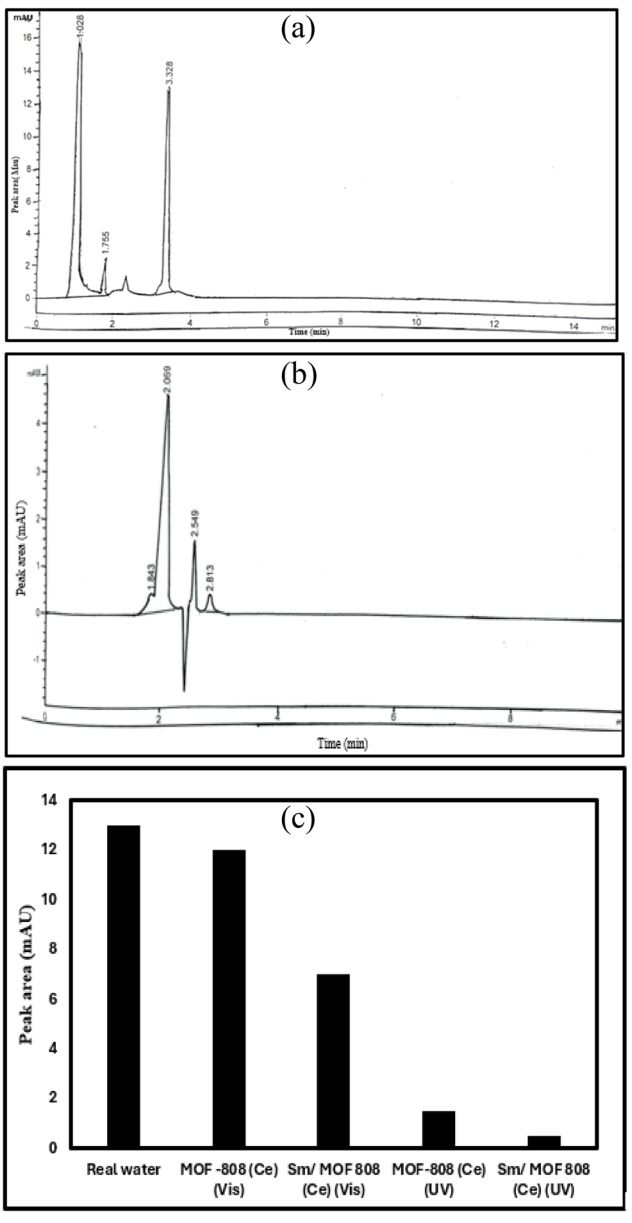

Fig. 10 (a) HPLC chromatograms of real sample containing famotidine (retention time 1.028 min) chlorpheniramine at 1.755 min and cefaclor (retention time of 3.328 min). (b) HPLC chromatograms of real sample under ultraviolet light with Sm/MOF-808(Ce). (c) Concentration of cefaclor in real wastewater sample in visible and ultraviolet light.

Table 2 Performance of some MOF based composites as photocatalysts for degradation of drugs

MOF based composite	Pollutant	Degradation efficiency (%)	Time (min)	References
MOF-5	Tetracycline	96	60	65
Bi_2S_3/MOF-808	Tetracycline	80.8	60	66
CuO@C	Paracetamol	95	60	67
$NiCo_2O_4$@MOF-801@MIL-88A	Meropenem	99	45	68
Ti–MOF	Tetracycline (TC)	87.03	60	69
	Chlortetracycline (CTC)	78.91		
MHACF–MOF-808(Zr)	Sulfamethazine	21	180	70
AgI/MOF-808	Tetracycline hydrochloride (TCH)	83.02	60	71
NH_2–UiO-66	Ketorolac tromethamine	68.6	120	72
	Tetracycline	71.8		
Sm/MOF-808(Ce)	Cefaclor	99.25	20	Current work

degradation in UV and visible light for different models are presented in Table 1. The table depicted 50% confidence region critical boundary value *i.e.* S_c. The critical values of S_c are less than S_{SFO} values. So, the SFO model cannot not be fitted to dissipation of cefaclor as per guidelines of NAFTA. In this case it is preferable to use DFOP or IORE model for degradation of cefaclor. The preference will be given on the basis of T_{IORE} value for IORE model and DT50 value of DFOF model.

T_{IORE} values are less than 2DT50. So, degradation of cefaclor followed DFOP kinetics and it can be used to determine the half-life of cefaclor. MOF-808(Ce) tested under the same reaction conditions exhibited the greater light harvesting at surface of the doped MOF in the UV-visible range. The half-life value of cefaclor degradation with Sm/MOF-808(Ce) (693 min) is less than MOF-808(Ce) (816 min) in visible light. Similarly in UV light, the half value of cefaclor with Sm/Ce-MOF-808 (88 min) is less than MOF-808(Ce) *i.e.*, (693 min). According to these results Sm/MOF-808(Ce) has the greatest photodegradation efficiency and higher rate kinetics for cefaclor degradation in UV light.

Photodegradation experiments conducted on real water sample containing cefaclor and other drugs were used to test the efficiency of prepared catalyst in real system applications as shown in HPLC graphs of Fig. 10. It was observed that the peak areas was decreased with the increase in degradation as compared to the peak areas of same concentration of the non-degraded cefaclor. Moreover, no additional peaks of degradation intermediates were observed showing complete degradation of cefaclor. The chromatograms showed that under visible light irradiation, cefaclor concentration was observed to be decreased. While, in the presence of UV light, no cefaclor peak was detected after only 30 minutes of irradiation indicating that photocatalytic degradation was complete and cefaclor was degraded completely without the production of any hazardous intermediate.

Table 2 provides a comparison of photo-catalytic degradation of different drugs by using MOFs and MOF based composites. Chen *et al.* (2022) used $NiCo_2O_4$@MOF-801@MIL-88A for the 99% photodegradation of meropenum in 45 minutes. Another study reported the 95% degradation of paracetamol in only 60 minutes. Among all the catalyst, the Sm doped MOF-808(Ce) was found to be the most efficient one, that degraded 99.25% cefaclor drug completely in 20 minutes. Thus, the prepared catalyst may be used for the removal of hazardous micropollutants from wastewaters in short interval of time, thereby ensuring a safe and clean environment.

4 Conclusions

MOF-808(Ce) and its functionalized form Sm/MOF-808(Ce) were prepared and used for the photocatalytic degradation of cefaclor. The materials were synthesized by using a simple facile method. The data for photodegradation studies showed that 97.58% cefaclor was completely mineralized in only 20 minutes at a pH of 4 by using Sm/MOF-808(Ce). While 99% removal was achieved within 60 minutes. The kinetic studies of MOFs suggested that removal of drug from wastewater followed and IORE kinetics. The newly constructed metal organic framework is a promising candidate for drug degradation in wastewater as it efficiently reduced the half-life of the cefaclor. The half-life was reduced from 693.3 min to 88 min in UV radiation. Furthermore, activating the MOF using ultraviolet light improves the structural, and morphological properties for enhanced selective drug affinity. The use of free radical scavengers verified that all $^{\bullet}OH$, h^+, e^- or $^{\bullet}O_2^-$ were responsible for the process of photodegradation.

So, the synthesized MOF may be used for the decontamination of wastewater without any ecotoxic intermediates. The prepared materials may be explored with respect to their effectiveness for the complete degradation of other hazardous micro-pollutants present in contaminated water effluents.

Author contributions

Anum Khaleeq: methodology, data curation, formal analysis, investigation, writing-original draft. Saadia Rashid Tariq: conceptualization, visualization, supervision, administration, revisions, and editing. Ghayoor Abbas Chotana: instrumental facilities for material characterization, resources.

Conflicts of interest

The authors declare that they have no known competing interest to declare.

Acknowledgements

The authors are thankful to Lahore College for Women University, Lahore for providing support for purchase of chemicals and glassware for this research work.

References

1 Â. Almeida, V. Calisto, V. I. Esteves, R. J. Schneider, A. M. Soares, E. Figueres and R. Freitas, *Aquat. Toxicol.*, 2014, **156**, 74–87.
2 T. Brodin, J. Fick, M. Jonsson and J. Klaminder, *Science*, 2013, **339**, 814–815.
3 D. Awfa, M. Ateia, M. Fujii, M. S. Johnson and C. Yoshimura, *Water Res.*, 2018, **142**, 26–45.
4 N. J. Vickers, *Curr. Biol.*, 2017, **27**, 713–715.
5 J. L. Wilkinson, A. B. A. Boxall, D. W. Kolpin, K. M. Y. Leung, R. W. S. Lai, D. Wong and H. Kang, *Proc. Natl. Acad. Sci. U. S. A.*, 2022, **119**, 1–10.
6 L. V. Trong, N. T. T. Hang, D. Q. Huy, N. M. Khai and T. V. Son, *Vietnam J. Chem.*, 2019, **57**, 234–239.
7 L. Niemi, P. Landová, M. Taggart, K. Boyd, Z. Zhang and S. Gibb, *Environ. Pollut.*, 2022, **292**, 118295.
8 S. Lockwood, N. Saïdi and V. A. Morgan, *The public expert for controlling industrial and environmental risks*, INERIS French National Institute for Industrial Environment and Risks, 2016.
9 T. Rasheed, M. Bilal, A. A. Hassan, F. Nabeel, R. N. Bharagava, L. F. R. Ferreira and H. M. Iqbal, *Environ. Res.*, 2020, **185**, 109436.
10 D. B. Hernández-Uresti, A. Vázquez, D. Sanchez-Martinez and S. Obregón, *J. Photochem. Photobiol., A*, 2016, **324**, 47–52.
11 J. E. Sosa-Hernández, L. I. Rodas-Zuluaga, I. Y. López-Pacheco, E. M. Melchor-Martínez, Z. Aghalari, D. S. Limón and R. Parra-Saldívar, *Case Stud. Chem. Environ. Eng.*, 2021, **4**, 100127.
12 M. T. Sekulic, N. Boskovic, M. Milanovic, N. G. Letic, E. Gligoric and S. Pap, *J. Mol. Liq.*, 2019, **284**, 372–382.
13 X. Chen, X. Peng, L. Jiang, X. Yuan, J. Fei and W. Zhang, *Chem. Eng. J.*, 2022, **427**, 130945.
14 L. Wang, P. Chen, X. Dong, W. Zhang, S. Zhao, S. Xiao and Y. Ouyang, *RSC Adv.*, 2020, **10**, 44687.
15 N. Prasetya and K. Li, *Chem. Eng. J.*, 2021, **417**, 129216.
16 G. Wang, T. Sun, Z. Sun and X. Hu, *Appl. Surf. Sci.*, 2020, **532**, 147411.
17 G. Crini and E. Lichtfouse, *Environ. Chem. Lett.*, 2019, **17**, 145–155.
18 M. Hu, J. Liu, S. Song, W. Wang, J. Yao, Y. Gong and Z. Li, *ACS Catal.*, 2022, **12**, 3238–3248.
19 M. A. Al-Nuaim, A. A. Alwasiti and Z. Y. Shnain, *Chem. Pap.*, 2023, **77**, 677–701.
20 S. Duan, J. Li, X. Liu, Y. Wang, S. Zeng, D. Shao and T. Hayat, *ACS Sustain. Chem. Eng.*, 2016, **4**, 3368–3378.
21 Z. Luo, S. Fan, J. Liu, W. Liu, X. Shen, C. Wu and M. Zheng, *Polymers*, 2018, **10**, 209.
22 L. Zhang, J. S. Sun, F. Sun, P. Chen, J. J. Liu and G. Zhu, *Chem.–Eur. J.*, 2019, **25**, 3903–3908.
23 R. Zhao, Y. Tian, S. Li, T. Ma, H. Lei and G. Zhu, *J. Mater. Chem. A*, 2019, **7**, 22559–22570.
24 L. Zhang, J. S. Sun, F. Sun, P. Chen, J. Liu and G. Zhu, *Chem.–Eur. J.*, 2019, **25**, 3903–3908.
25 R. Muruganantham, Y. J. Gu, Y. D. Song, C. W. W. Kung and W. R. Liu, *Appl. Mater. Today*, 2021, **22**, 100935.
26 M. E. Awad, A. M. Farrag, A. A. El-Bindary, M. A. El-Bindary and H. A. Kiwaan, *Appl. Organomet. Chem.*, 2023, e7113.
27 L. Hu, J. Chen, Y. Wei, M. Wang, Y. Xu, C. Wang and R. Wang, *J. Hazard. Mater.*, 2023, **442**, 130059.
28 R. Kaur, A. Kaur, R. Kaur, S. Singh, M. S. Bhatti, A. Umar and S. K. Kansal, *Adv. Powder Technol.*, 2021, **32**, 1350–1361.
29 D. Mohan, A. Sarswat, Y. S. Ok and C. U. Pittman Jr, *Bioresour. Technol.*, 2014, **160**, 191–202.
30 K. G. Laurier, F. Vermoortele, R. Ameloot, D. E. De Vos, J. Hofkens and M. B. Roeffaers, *J. Am. Chem. Soc.*, 2013, **135**(39), 14488–14491.
31 Y. Li, J. Jiang, Y. Fang, Z. Cao, D. Chen, N. Li and J. Lu, *ACS Sustain. Chem. Eng.*, 2018, **6**, 16186–16197.
32 R. Zhao, Y. Tian, S. Li, T. Ma, H. H. Lei and G. Zhu, *J. Mater. Chem. A*, 2019, **7**, 22559–22570.
33 R. Banerjee, A. Phan, B. Wang, C. Knobler, H. Furukawa, M. O'Keeffe and O. M. Yaghi, *Science*, 2008, **319**, 939–943.
34 Y. Zhang, S. Yuan, X. Feng, H. Li, J. Zhou and B. Wang, *J. Am. Chem. Soc.*, 2016, **138**, 5785–5788.
35 M. Samy, M. G. Ibrahim, M. Fujii, K. E. Diab, M. M. ElKady and M. G. Alalm, *Chem. Eng. J.*, 2021, **406**, 127152.
36 J. Kujawa, S. Al-Gharabli, T. M. Muzioł, K. Knozowska, G. Li, L. F. Dumee and W. Kujawski, *Coord. Chem. Rev.*, 2021, **440**, 213969.
37 X. Jiong, L. Zhen, W. Xianbiao, X. Yongfei, C. Saisai and W. Zhuo, *New J. Chem.*, 2019, **10**, 1–21.
38 A. J. Watkinson, E. J. Murby and S. D. Costanzo, *Water Res.*, 2007, **41**, 4164–4176.
39 J. M. Yassin, A. M. Taddesse and M. Sanchez-Sanchez, *Microporous Mesoporous Mater.*, 2021, **324**, 111303.
40 S. Sundararaman, J. A. Kumar, P. Deivasigamani and Y. Devarajan, *Sci. Total Environ.*, 2022, **825**, 153897.
41 R. Muruganantham, Y. J. Gu, Y. D. Song, C. W. Kung and W. R. Liu, *Appl. Mater. Today*, 2021, **22**, 100935.
42 W. Wang, S. Song, P. Wang, M. He, Z. Fang, X. Yuan and Z. Li, *ACS Catal.*, 2023, **13**, 4597–4610.
43 Z. Shayegan, F. Haghighat and C. S. Lee, *Chem. Eng. J.*, 2020, **401**, 125932.
44 D. Ma, Y. Li and Z. Li, *Chem. Commun.*, 2011, **47**, 7377–7379.
45 A. Bakhtiar, Z. Bouberka, P. Roussel, C. Volkringer, A. Addad, B. Ouddane, C. Pierlot and U. Maschke, *Nanomaterials*, 2022, **12**, 3313.
46 S. Bagi, S. Yuan, S. R. Buzo, Y. Shao-Horn and Y. Roman-Leshkov, *Green Chem.*, 2021, **23**, 9982–9991.
47 S. Lin, Y. Zhao and Y. S. Yun, *ACS Appl. Mater. Interfaces*, 2018, **10**, 28076–28085.
48 Y. Guo, X. Zhang, N. Xie, R. Guo, Y. Wang, Z. Sun and H. B. Sun, *Dalton Trans.*, 2021, **50**, 13932–13942.
49 K. Divakaran, A. Baishnisha, V. Balakumar, K. N. Perumal, C. Meenakshi and R. S. Kannan, *J. Environ. Chem. Eng.*, 2021, **9**, 105560.

50 S. Yu, G. Yuan, H. Gao and Y. Liao, *J. Mater. Sci.*, 2022, **55**, 163–176.
51 M. E. Argun, *J. Hazard. Mater.*, 2008, **150**(3), 587–595.
52 H. T. Nguyen Thi, K. N. Tran Thi, N. B. Hoang, B. T. Tran, T. S. Do, C. S. Phung and K. O. Nguyen Thi, *Materials*, 2021, **14**, 7741.
53 L. A. Lozano, L. A. S. Hoyos, B. M. M. Faroldi and J. M. Zamaro, *Mater. Today Commun.*, 2022, **31**, 103540.
54 T. H. Do, N. Q. Dung, M. N. Chu, D. Van Kiet, T. T. K. Ngan and L. Van Tan, *Mater. Today: Proc.*, 2021, **38**, 3405–3413.
55 L. Jing, W. Zhou, G. Tian and H. Fu, *Chem. Soc. Rev.*, 2013, **42**, 9509–9549.
56 W. Mohammed, M. Matalkeh, R. M. Al Soubaihi, A. A. Elzatahry and K. M. Saoud, *ACS Omega*, 2023, **8**(43), 40063–40077.
57 J. Tang and J. Wang, *Chem. Eng. J.*, 2018, **351**, 1085–1094.
58 J. Chang, S. Yu, Y. Liao, X. Guan, H. Gao and Y. Li, *ACS Omega*, 2022, **7**, 42854–42864.
59 C. Yang, Z. Xue and J. Wen, *Sustainability*, 2023, **15**, 6686.
60 M. He, Z. Fang, P. Wang, Y. You and Z. Li, *ACS Sustain. Chem. Eng.*, 2023, **11**, 12194–12217.
61 S. R. Morrison and S. R. Morrison, *Electrochemistry at semiconductor and oxidized metal electrodes*, Plenum Press, New York, 1980, vol. 126, p. 246.
62 X. Li and J. Ye, *J. Phys. Chem. C*, 2007, **111**, 13109–13116.
63 S. Khuntia, S. K. K. Majumder and P. Ghosh, *Environ. Technol.*, 2015, **36**, 336–347.
64 S. Yu, Q. Wang, J. Wang, C. Fang, Y. Li, J. Ge and B. Fang, *Catal. Sci. Technol.*, 2023, 6583–6603.
65 S. M. Mirsoleimani-azizi, P. Setoodeh, S. Zeinali and M. Rahimpour, *J. Environ. Chem. Eng.*, 2018, **6**, 6118–6130.
66 F. Wang, R. Xue, Y. Ma, Y. Ge, Z. Wang, X. Qiao and P. Zhou, *RSC Adv.*, 2021, **11**, 32955–32964.
67 A. Abdelhaleem, H. N. Abdelhamid, M. G. Ibrahim and W. Chu, *J. Cleaner Prod.*, 2022, **379**, 134571.
68 M. Bakhtian, N. Khosroshahi and V. Safarifard, *ACS Omega*, 2022, **7**, 42901–42915.
69 X. Chen, X. Peng, L. Jiang, X. Yuan, J. Fei and W. Zhang, *Chem. Eng. J.*, 2022, **427**, 130945.
70 W. J. Qiu, M. W. Gao, Q. Chen, A. Zheng, Y. J. Shi, X. Liu and Z. X. Lin, *Appl. Organomet. Chem.*, 2022, **36**, e6556.
71 Y. Dong, X. Wang, H. Sun, H. Zhang, X. Zhao and L. Wang, *Chem. Eng. J.*, 2023, **460**, 141842.
72 M. Kaur, S. K. Mehta and S. K. Kansal, *Environ. Sci. Pollut. Res.*, 2023, **30**, 8464–8484.